Supplementary

Perovskite Ionics - Elucidating Degradation Mechanisms in Perovskite Solar Cells via Device Modelling and Iodine Chemistry

Sapir Bitton and Nir Tessler*
Sara and Moshe Zisapel Nano-electronic centre, Electrical and Computer Electronics,
Technion Israel Institute of Technology

I. The chemical physics picture captured by the device simulations

To motivate the reader to dive into our discussion below, we state that **our model has been verified** with experimental results and has assisted in extracting a more profound understanding from such data. [1-4] The simulation is based on a standard semiconductor device model that can describe various device structures based on electrons and holes. We have added cations (positive ions) and anions (negative ions) to this. In $MAPbI_3$ perovskite, several ionic defects could be associated with the constituents of the crystal [5] and treating them in a self-consistent manner is of the essence. For the species transport, we use the following set of equations (we employ the general nomenclature found in the Sentaurus manual):

The transport equations for the iodine atom (X_1), the I_2 molecule (X_2), and the iodide ion (X_3) can be written as:

$$(1)\ \frac{\partial}{\partial t}[X_i] + \nabla \cdot D_i \exp\left(-\frac{E_{A\,i}}{k_B T}\right)\left(\frac{qK_i^Q}{k_B T}F[X_i] - \nabla[X_i]\right) + R_{net} = 0$$

Where: D_i is the diffusion coefficient; $E_{A\,i}$ is the activation energy; K_i^Q is the number of charges for element X; R_{net} is the net recombination rate due to chemical reactions.

The chemical reactions between mobile elements, with N different elements, can be described by the following equation:

$$(2)\qquad \sum_{i=1}^{N} \alpha_i X_i \leftrightarrow \sum_{i=1}^{N} \beta_i X_i$$

Where X_i can be atoms, molecules, ions, electrons, and holes. α_i and β_i are the particle numbers of elements X_i participating in the reaction.

In our case $N = 5$. The elements are three iodine species - $I,\ I_2, I^-$ and electronic charges - $e^-, and\ h^+$. So, equation (2) must comply with the conservation law of charge and iodine:

(3) $$\sum_{i=1}^{5}(\alpha_i - \beta_i)K_i^Q = 0$$

(4) $$\sum_{i=1}^{5}(\alpha_i - \beta_i)K_i^H = 0$$

Where K_i^Q and K_i^H are the number of charges and number of iodine atoms for element X_i.

The forward and reverse reaction rates, R_f and R_r , are modeled as:

(5) $$R_f = k_f \prod_{i=1}^{5}\left(\frac{[X_i]}{cm^{-3}}\right)^{\alpha_i}$$

(6) $$R_r = k_r \prod_{i=1}^{5}\left(\frac{[X_i]}{cm^{-3}}\right)^{\beta_i}$$

Where k_f and k_r are the forward and reverse reaction coefficients respectively ($(cm^{-3}s^{-1})$ for bulk reaction and $(cm^{-2}s^{-1})$ for interface reaction).

I.A. Which defect pair is relevant?

Assuming that the crystal is perfect and stoichiometric at low temperatures, we can expect to find room-temperature Frenkel defect pairs. [5] If a component exits the crystal structure, it forms an interstitial defect (Ma_i, Pb_i, I_i) that leaves behind the corresponding vacancy (V_{MA}, V_{Pb}, V_I). [6] In our model, positive defects are counted using n_c and negative ones are n_a. For simplicity, we make the common assumption and consider only **iodine species**. [7] We wrote "for simplicity" since, for example, there is evidence that Pb ions could be mobile too. [8]

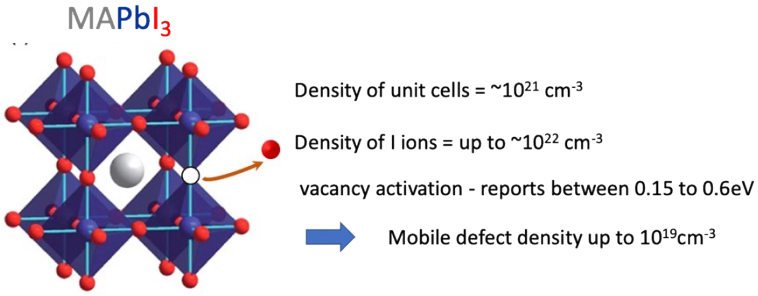

Illustration of the formation of vacancy-interstitial Frenkel pair defects and the predicted defect density.

I.B. Which defect is mobile?

If we consider only iodine species, then it should be clear that only iodide is moving. Similarly to standard semiconductors, if the iodide is outside the crystal lattice, we say an interstitial iodide (I_i) moved (as do electrons in the conduction band). Suppose the iodide is moving within the crystal lattice. In that case, it is common to describe it as an iodide vacancy (V_I) motion (as holes describe

the motion of electrons within the valence band). In standard semiconductors, when a heterostructure is created, electrons and holes can cross the interface; hence, it is essential to account for both. However, all the early modelling efforts assumed that the defects were confined to the perovskite layer making it less critical to account for the motion of both charged defects. In such a case, the model's primary goal is to simulate the motion of a charged defect and ensure that the overall charge neutrality is preserved. We found that using only the J-V curves of measured devices, the model cannot distinguish between the motion of positive, negative, or both defects. Indeed, we and others started by modelling the motion of positive defects (as iodide vacancies) [7, 9] while keeping a fixed density of negative defects (as iodide interstitials). However, we recently participated in a 3-group effort to explain measured excitation-induced band bending and over stoichiometric concentration of iodides. [3] We had to opt for iodide motion to reproduce the nm scale band bending. The choice of parameters was driven by DFT calculations confirming excess iodide formation. [3] Moreover, as we started to model iodide diffusion into the blocking layers, [10, 11] it was clear that we had to account for mobile iodides.

We do not claim that iodides do not move within the crystal framework but rather that we must account for their motion outside the crystal lattice. This is why we do not mark the moving iodide as an interstitial defect (I_i^-) nor as a vacancy (V_I), but simply as I^-.

To conclude this subsection, using JV analysis only, we could not justify using two mobile ions. UPS-XPS measurements and DFT calculations drove us to include iodide diffusion. This implies that for the model to be good enough, it must include a background of positive defects to maintain overall charge neutrality.

I.C. What is the defect density?

As the figure above indicates, the unit cell is slightly below 1nm cube[12], making the iodine density in the 10^{22}-10^{23}cm^{-3} range. The defect formation energy has a spread of values in the literature and depends on the defect's position relative to the grain boundaries. [13] Namely, a literature report could justify any number up to 10^{19}cm^{-3}. The lower bound is dictated by these mobile ions introducing electrostatic effects in the form of band bending. We found minimal effects for average defect density below 10^{17}cm^{-3}, so we consider 10^{17}-10^{19}cm^{-3} as a reasonable range. The actual number we use is 10^{18} cm^{-3}.

I.D. Ion diffusion coefficient in the perovskite

The ion diffusion coefficient within the perovskite layer is estimated between 10^{-9} and $10^{-6}\frac{cm^2}{s}$. [14, 15] Our choice of 10^{-8} is within the well-accepted values.

I.E. Ion diffusion coefficient in the blocking layers

There is no information we can rely on regarding the ion diffusion within the blocking layers. It is known that ionic motion is affected by the layer's density (or "free space") and by the rigidity of the structure. The blocking layers used are anywhere between polycrystalline C_{60}, amorphous oxides, or conjugated polymers, so there is no "one size fits all". It is reasonable to assume that for devices that do not degrade within an hour, the ions' diffusion in the blocking layer is slower than their diffusion within the perovskite layer. If it is lower by at least an order of magnitude, we can consider the diffusion within the perovskite and the blocking layers to be on different time scales such that one can distinguish between them. We chose 4 orders of magnitude difference to mimic devices that do not degrade too fast. The actual conclusions we draw do not depend on the time it takes the device to degrade. We are only interested in the degradation mechanisms.

I.F. Reactions and reactions rates

Here too, we have no independent data to rely on. To maintain consistency within the model framework, we assume that the reactions are diffusion limited. Namely, the choice of diffusion coefficients dictates the reaction rates. The best minimal set of reactions is not determined in the literature either. We opted for one readily implemented within the model framework, forming a close cycle supporting the healing phenomena (see main text). Considering the conclusions drawn using our reactions set, we note that the effect of iodide interstitial acting as a recombination centre is supported by DFT calculations, [6] and the formation of I_2 gas has been suggested before. [16, 17]

I.G. The parameters used in the simulations

Table S1. The parameters used in the solar cells' simulation. The reactions were calculated using $R_{AB} = 0.2nm$.

	Perovskite	HBL	EBL
Layer thickness (nm)	500	50	50
Affinity, $\chi(eV)$	4.3	4.3	3.4
Band gap, $E_g(eV)$	1.6	2.5	2.5
Charge mobility, $\mu_e = \mu_h \left(\frac{cm^2}{V \cdot sec}\right)$	2	$10^{-3}; 10^{-4}$	$10^{-3}; 10^{-4}$
Dielectric constant, ε_r	50	3	3
Conduction density of states (cm^{-3})	$7 \cdot 10^{18}$	10^{21}	10^{21}
Valence density of states (cm^{-3})	$2.5 \cdot 10^{18}$	10^{21}	10^{21}

Initial I^- and I vacancy density $\left(cm^{-3}\right)$	10^{18}	*0*	*0*
Ion I^- diffusion $\left(\frac{cm^2}{s}\right)$	10^{-8}	10^{-12}	10^{-12}
Atom I diffusion $\left(\frac{cm^2}{s}\right)$	10^{-8}	10^{-12}	10^{-12}
Molecule I_2 diffusion $\left(\frac{cm^2}{s}\right)$	10^{-9}	10^{-13}	10^{-13}
Radiative recombination $\left(\frac{cm^3}{s}\right)$	10^{-10}	Langevin	Langevin
Reaction rate - $I^- + h \rightarrow I$ $\left(\frac{cm^3}{s}\right)$	10^{-11} ; 5x10^{-11}	$6.5 \cdot 10^{-13}$	$6.5 \cdot 10^{-13}$
Reaction rate - $I \rightarrow I^- + h$ $\left(\frac{cm^3}{s}\right)$	$3 \cdot 10^5$	$6 \cdot 10^3$	$6 \cdot 10^{-12}$
Reaction rate - $I + e_{E_C} \rightarrow I^-$ $\left(\frac{cm^3}{s}\right)$	$5 \cdot 10^{-7}$	$2.5 \cdot 10^{-11}$	$2.5 \cdot 10^{-11}$
Reaction rate - $2I \rightarrow I_2$ $\left(\frac{cm^3}{s}\right)$	$5 \cdot 10^{-15}$	$5 \cdot 10^{-19}$	$5 \cdot 10^{-19}$
Reaction rate - $I_2 + 2e \rightarrow 2I^-$ $\left(\frac{cm^3}{s}\right)$	$1.3 \cdot 10^{-8}$	$1.3 \cdot 10^{-10}$	$1.3 \cdot 10^{-10}$

II. Additional figures

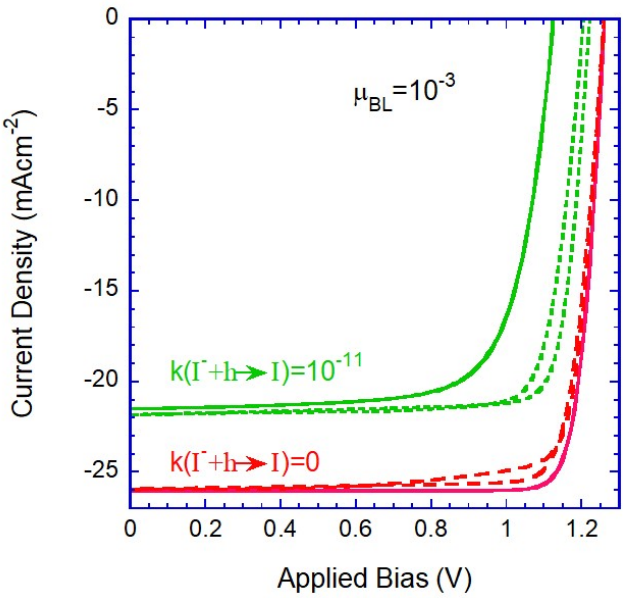

Figure S1. JV characteristics for hysteresis scan were obtained after the devices were held under one Sun and 0.9V to reach a steady state. The electron and hole mobility in the blocking layer was $10^{-3}cm^2V^{-1}s^{-1}$. The different line colours are for no ion reactions (red), and a hole-trapping rate of 10^{-11} (green). Full and dashed lines are for the blocking layers being blocking and permeable to ions, respectively.

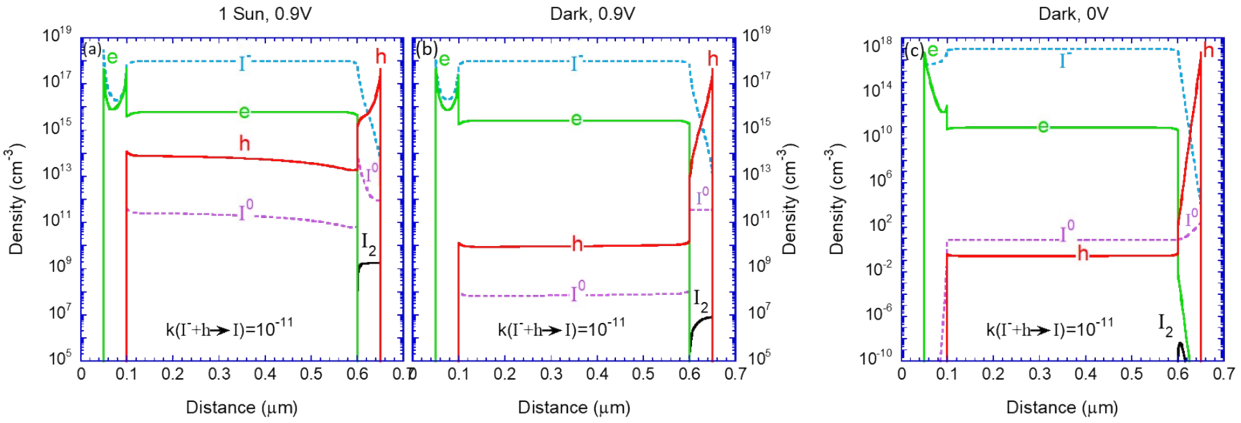

Figure S2. The electronic charges and the iodine species distribution after the stress period at 0.9V and under 1Sun (a) and dark (b) conditions. (c) The device is in short-circuit and dark (note the different y-scale). The reactions are on, and the BLs are permeable.

References

1. H. Shekhar, V. Lami, O. Solomeshch, A. Fenigstein, L. Tomer, L. Becky, Y. Vaynzof and N. Tessler, Organic Electronics **67**, 1-9 (2019).
2. Q. An, F. Paulus, D. Becker-Koch, C. Cho, Q. Sun, A. Weu, S. Bitton, N. Tessler and Y. Vaynzof, Matter **4** (5), 1683-1701 (2021).
3. J. A. Kress, C. Quarti, Q. An, S. Bitton, N. Tessler, D. Beljonne and Y. Vaynzof, ACS Energy Letters **7** (10), 3302-3310 (2022).
4. F. Zu, M. Roß, L. Frohloff, D. Shin, N. Tessler, S. Albrecht and N. Koch, Solar RRL, 2101065 (2022).
5. D. Meggiolaro, S. G. Motti, E. Mosconi, A. J. Barker, J. Ball, C. Andrea Riccardo Perini, F. Deschler, A. Petrozza and F. De Angelis, Energy Environ. Sci. **11** (3), 702-713 (2018).
6. S. G. Motti, D. Meggiolaro, S. Martani, R. Sorrentino, A. J. Barker, F. De Angelis and A. Petrozza, Advanced Materials **31** (47), 1901183 (2019).
7. G. Richardson, S. E. J. O'Kane, R. G. Niemann, T. A. Peltola, J. M. Foster, P. J. Cameron and A. B. Walker, Energy Environ. Sci. **9** (4), 1476-1485 (2016).
8. S. T. Birkhold, J. T. Precht, H. Liu, R. Giridharagopal, G. E. Eperon, L. Schmidt-Mende, X. Li and D. S. Ginger, ACS Energy Letters **3** (6), 1279-1286 (2018).
9. N. Tessler and Y. Vaynzof, ACS Applied Energy Materials **1** (2), 676-683 (2018).
10. S. Bitton and N. Tessler, Applied Physics Letters **117** (13), 133904 (2020).
11. S. Bitton and N. Tessler, J. Mater. Chem. C **9** (6), 1888-1894 (2021).
12. M. T. Weller, O. J. Weber, J. M. Frost and A. Walsh, The Journal of Physical Chemistry Letters **6** (16), 3209-3212 (2015).
13. D. Meggiolaro, E. Mosconi and F. De Angelis, ACS Energy Letters **4** (3), 779-785 (2019).
14. S. Reichert, Q. An, Y.-W. Woo, A. Walsh, Y. Vaynzof and C. Deibel, Nature Communications **11** (1) (2020).
15. M. H. Futscher, J. M. Lee, L. McGovern, L. A. Muscarella, T. Wang, M. I. Haider, A. Fakharuddin, L. Schmidt-Mende and B. Ehrler, Materials Horizons **6** (7), 1497-1503 (2019).
16. L. Bertoluzzi, J. B. Patel, K. A. Bush, C. C. Boyd, R. A. Kerner, B. C. O'Regan and M. D. McGehee, Advanced Energy Materials **11** (10), 2002614 (2021).
17. J. Cho, J. T. Dubose, P. S. Mathew and P. V. Kamat, Chemical Communications **57** (2), 235-238 (2021).